[4] C. P. Keijzers, H. J. M. de Vries, and A. van der Avoird, Inorg. Chem. (to be published).
[5] W. Low, *Paramagnetic Resonance in Solids* (Academic, New York, 1960), p. 43.
[6] M. Bonamico, G. Dessy, C. Mariani, A. Vaciago, and L. Zambonelli, Acta Cryst. **19,** 619 (1965).
[7] J. G. M. van Rens, C. P. Keijzers, and H. van Willigen, J. Chem. Phys. **52,** 2858 (1970).
[8] An elaborate report will be published soon.
[9] M. Bonamico and G. Dessy, J. Chem. Soc. A **1971,** 264.
[10] J. Richardson, W. Nieuwpoort, R. Powell, and W. Edgell, J. Chem. Phys. **36,** 1057 (1962).
[11] J. Richardson, R. Powell, and W. Nieuwpoort, J. Chem. Phys. **38,** 796 (1963).
[12] E. Clementi and D. Raimondi, J. Chem. Phys. **38,** 2686 (1963).
[13] H. Basch, A. Viste, and H. B. Gray, Theoret. Chim. Acta **3,** 458 (1965).
[14] C. E. Moore, Natl. Bur. Stds. (U.S.) Circ. 467, Vol. I (1949); II (1952); and III (1958).
[15] J. S. Griffith, *The Theory of Transition-Metal Ions* (Cambridge, U. P., Cambridge, 1964), 2nd ed, p. 437.
[16] C. A. Bates, Proc. Phys. Soc. **79,** 69 (1962).
[17] A. Carrington and A. D. Mclachlan, *Introduction to Magnetic Resonance,* (Harper & Row, New York, 1967) 1st ed, p. 138.
[18] Calculated from Ref. 14.
[19] E. Clementi, IBM J. Res. Dev. Suppl. **9,** 2 (1965).

THE JOURNAL OF CHEMICAL PHYSICS VOLUME 57, NUMBER 3 1 AUGUST 1972

Molecular Dynamics Study of Temperature Effects on Water Structure and Kinetics*

FRANK H. STILLINGER
Bell Laboratories, Murray Hill, New Jersey 07974
AND
ANEESUR RAHMAN
Argonne National Laboratory, Argonne, Illinois 60439

(Received 13 April 1972)

For a system of 216 water molecules, molecular dynamics calculations have been carried out at two temperatures in addition to the one studied and reported previously. As before, the Ben-Naim and Stillinger effective pair potential was used for these calculations. The results document the breakdown of hydrogen-bond order and the rapid increase in the freedom of molecular motions that accompany temperature rise in real water. We find no evidence at any temperature to support those water models which partition molecules into two classes (bonded framework or cluster molecules vs unbonded molecules). Nevertheless the pair potential distribution function changes with temperature in such a way as to suggest a basic hydrogen-bond rupture mechanism characterized by an excitation energy of about 2.5 kcal/mole. Some results indicate that the potential utilized is a bit too tetrahedrally directional to represent real water faithfully, so a possible modification is mentioned.

I. INTRODUCTION

A molecular dynamics project was recently initiated[1] to investigate a classical dynamical model[2] for molecular arrangement and motions in liquid water. Our first report on this project was devoted primarily to results for the model liquid at just one temperature. In this article we shall explain how our subsequent numerical results reveal the effect of temperature changes (at fixed density) on both structural and kinetic aspects of the model.

From results of several independent quantum mechanical calculations[3–7] (coupled with prior crystallographic knowledge about aqueous crystal structures), useful detail about water molecule interaction energies is now available. The key feature involved is the tendency toward formation of linear hydrogen bonds between neighbors disposed in space in a tetrahedral coordination pattern. The quantum mechanical calculations also reveal that the intermolecular interactions are significantly nonadditive.[5,6]

Our waterlike model has employed the Ben-Naim and Stillinger "effective" pair potential,[2] which consists of a central Lennard-Jones component (appropriate for isoelectronic neon[8]), and an orientation-dependent part based upon a four-point charge complex within each water molecule,

$$V_{\rm eff}^{(2)}(\mathbf{x}_i, \mathbf{x}_j) = v_{\rm LJ}(r_{ij}) + S(r_{ij}) v_{\rm el}(\mathbf{x}_i, \mathbf{x}_j). \quad (1.1)$$

Here r_{ij} is the radial distance between oxygen nuclei, and $v_{\rm el}$ is the sum of all 16 Coulombic charge-pair interactions between the molecules. Each molecule contains two charges $+0.19e$ ("shielded protons") and two charges $-0.19e$ ("unshared electrons") arranged at the vertices of a regular tetrahedron with radius 1 Å, whose center is the oxygen nucleus. The switching function S continuously and differentiably interpolates between 0 at small r_{ij} and 1 at large r_{ij},[9]

$$\begin{aligned} S(r_{ij}) &= 0, && (0 \le r_{ij} \le R_L) \\ &= \frac{(r_{ij}-R_L)^2(3R_U-R_L-2r_{ij})}{(R_U-R_L)^3}, && (R_L \le r_{ij} \le R_U) \\ &= 1, && (R_U \le r_{ij} < \infty). \end{aligned} \quad (1.2)$$

TABLE I. Data relevant to strength rescaling of the potential. The units employed are T: degrees Kelvin (Centigrade equivalent in parentheses), D: 10^{-5} cm^2/sec, $N^{-1}\langle V_N\rangle$: kilocalories/mole

$\zeta=$	0.00	0.03	0.06	0.09
T_1	265(−8.2)	273(−0.2)	280.9(7.7)	288.9(15.7)
D(m.d.)	1.5	1.5	1.5	1.6
D(exptl)[a]	0.74	1.0	1.4	1.8
$N^{-1}\langle V_N\rangle$(m.d.)	−10.09	−10.40	−10.70	−11.00
$N^{-1}\langle V_N\rangle$(exptl)	−10.32	−10.23	−10.14	−10.05
T_2	307.5(34.3)	316.7(43.5)	326(52.8)	335.2(62)
D(m.d.)	4.2	4.3	4.3	4.4
D(exptl)[a]	2.9	3.4	4.0	4.8
$N^{-1}\langle V_N\rangle$(m.d.)	−9.18	−9.45	−9.73	−10.00
$N^{-1}\langle V_N\rangle$(exptl)	−9.85	−9.75	−9.64	−9.54
T_3	588(314.8)	605.6(332.4)	623.3(350.1)	640.9(367.7)
D(m.d.)	23	23	24	24
D(exptl)[b]	24	25	27	28
$N^{-1}\langle V_N\rangle$(m.d.)	−5.91	−6.09	−6.27	−6.44
$N^{-1}\langle V_N\rangle$(exptl)	...	...	...	...

[a] Reference 27.

[b] These estimates made on the basis of the Stokes–Einstein relation, using measured viscosities [K. H. Dudziak and E. U. Franck, Ber. Bunsenges. Physik. Chem. **70**, 1120 (1966)].

The presence of this function in $V_{\text{eff}}^{(2)}$ is important in establishing the correct "shape" in regions of strong pair interaction; it also quenches the spurious divergences of v_{el} that occur at small r_{ij} due to charge overlap.

The major advantage of the potential (1.1) is that it incorporates the linear hydrogen-bonding tendency between neighbors in a tetrahedral pattern; to that extent it agrees with quantum mechanical and crystallographic information. It is unrealistic however in being pairwise additive. Fortunately one can rely upon the variational definition of an effective pair potential[10] to incorporate the major structural influence of many-body interactions as modifications of a pair interaction from its strict two-body form. The interaction $V_{\text{eff}}^{(2)}$ in Eq. (1.1) is assumed to have this character.

With current electronic computer capabilities, the molecular dynamics simulation of a waterlike system of acceptable size (see below) runs rather slowly. Short-term expedients which speed up running times are therefore attractive. An expedient that has proved useful in our work is the suppression of forces and torques acting between molecules beyond a certain cutoff distance.[1] Although this formally introduces irreversibility into the classical dynamical equations, the resulting secular rise in temperature during a computer run seems to have modest magnitude, so that we feel confident in quoting kinetic temperature averaged over the run as being physically relevant.

In the future, presuming that interest in these calculations persists, the advent of more powerful computers should permit more satisfactory modeling for liquid water. Not only will it be possible in principle to utilize explicit three-body, four-body, ..., interactions, but cutoffs and inherent irreversibility should be unnecessary. It is important to stress that our current expedients do not represent future restrictions of principle on the powerful molecular dynamics technique.

So far as fitting selected experimental data on water is concerned, the effective pair interaction (1.1) would not *a priori* be expected to prove optimal. In the following we shall therefore consider a rescaling of the strength of $V_{\text{eff}}^{(2)}$ by a factor $1+\zeta$. This does not affect the qualitative nature of the linear hydrogen bonding inherent in the interaction. Since the dynamical equations are solved in dimensionless form, the effect of this rescaling is very simple: Time intervals required

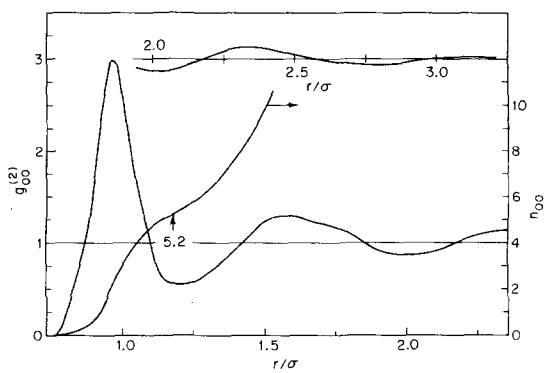

FIG. 1. Radial pair correlation function $g_{OO}^{(2)}$ for water at the low temperature T_1 and mass density 1 g/cm^3. The distance unit σ is 2.82 Å. The running coordination number $n_{OO}(r)$ refers to the scale at the right.

for given dynamical sequences contract by a factor $(1+\zeta)^{-1/2}$, while the absolute temperature increases by a factor $(1+\zeta)$.

As before, our calculations involve 216 molecules confined to a cubical cell of edge length 18.62 Å. At each temperature, then, the sample has the same mass density 1 g/cm³. By virtue of periodic boundary conditions, we eliminate the specific influence of container walls which would otherwise surely pose a severe problem in such a small system. Although it is also important to investigate the effect of varying the density, we reserve that aspect for later study.

For further details about our use of the molecular dynamics technique, the interested reader should consult Ref. 1.

II. TEMPERATURE VARIATION OF STATIC STRUCTURE

Molecular dynamics runs have been completed at three different temperatures, T_1, T_2, and T_3. The first

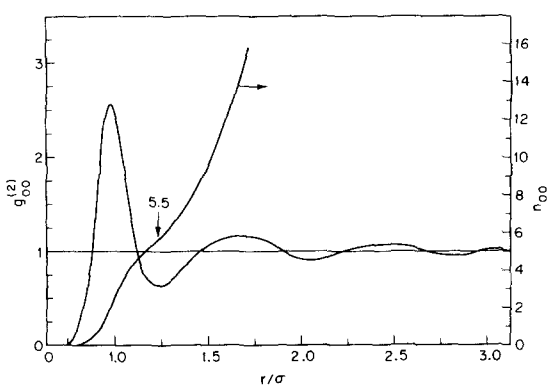

FIG. 2. Radial pair correlation function $g_{OO}^{(2)}$ and the corresponding running coordination number n_{OO} at intermediate temperature T_2 and mass density 1 g/cm³.

of these, T_1, corresponds to slightly supercooled water at 265°K (−8.2°C) if the interaction (1.1) is unscaled. Similarly the unscaled value for temperature T_2 is 307.5°K (34.3°C); the data obtained at this temperature formed the basis for Ref. 1 and are partially repeated here for comparison. The highest of the three temperatures T_3 has an unscaled value 588°K (314.8°C). This last state provides a concrete example of the importance of the molecular dynamics approach to simulate condensed matter under experimentally impractical circumstances, for besides being very hot the "water" sample at 1 g/cm³ would have a pressure around 6 kbar.[11]

Table I provides a set of scaled temperature identifications for T_1, T_2, and T_3 when the fractional coupling strength increase ζ takes on values 0.03, 0.06, and 0.09. This table also contains entries, connected with a later discussion, bearing on the optimal choice of ζ.

For the dynamical computations it is convenient to

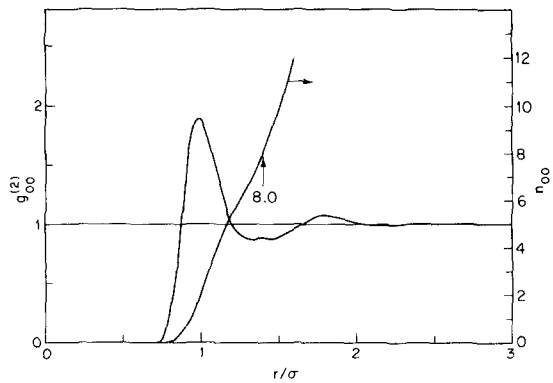

FIG. 3. High temperature (T_3) radial pair correlation function $g_{OO}^{(2)}$ and associated running coordination number n_{OO}. The mass density is 1 g/cm³.

measure time in units

$$t_0=\sigma(m/\epsilon)^{1/2}, \tag{2.1}$$

where m is the molecular mass, and σ and ϵ are the Lennard-Jones parameters for Ne.[8] The numerical integration for the T_1 and T_2 runs employed time increments,

$$\Delta t=2\times10^{-4}t_0=4.355\times10^{-16}\text{ sec}, \tag{2.2}$$

while the high temperature T_3 run required increments half as large. The total runs in each case lasted

$$\begin{aligned} T_1&:\quad 4000\Delta t=1.742\times10^{-12}\text{ sec},\\ T_2&:\quad 5000\Delta t=2.178\times10^{-12}\text{ sec},\\ T_3&:\quad 4755\Delta t=1.036\times10^{-12}\text{ sec}. \end{aligned} \tag{2.3}$$

Pair forces and torques were cut off in the T_1, T_2, and T_3 runs, respectively, at 3.25σ, 3.25σ, and 3.00σ.

A. Radial Pair Correlation Functions

The radial pair correlation functions $g_{OO}^{(2)}(r, T)$ for oxygen nuclei are exhibited in Figs. 1–3. The temperature-induced structural shifts are most obvious from the diminishing amplitudes of oscillations about asymp-

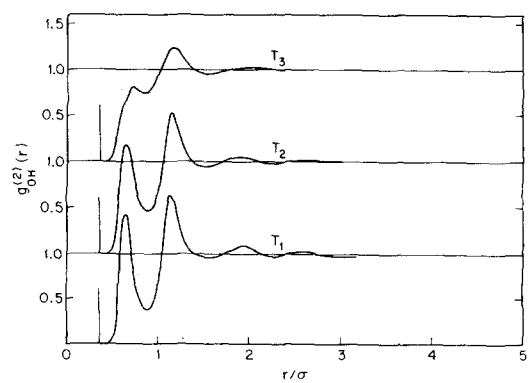

FIG. 4. Radial cross correlation function $g_{OH}^{(2)}(r)$ at the three temperatures T_1, T_2, T_3. The vertical line indicates the intramolecular O–H distance.

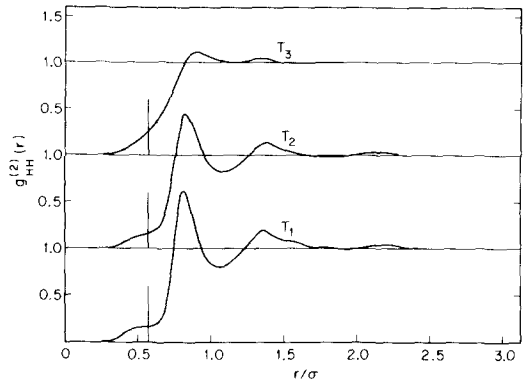

FIG. 5. Radial correlation function $g_{HH}^{(2)}(r)$ for protons at T_1, T_2, and T_3. The vertical line indicates the intermolecular H–H distance.

totic value unity, as T increases from T_1 (Fig. 1) to T_3 (Fig. 3). It is also obvious that the range of correlation declines with increasing T.

The running coordination numbers $n_{OO}(r)$, giving the average number of neighbors out to distance r, are also included in Figs. 1–3. At the respective distances of the first $g_{OO}^{(2)}$ minima, the computed numbers of "nearest neighbors" are $5.2(T_1)$, $5.5(T_2)$, and $8.0(T_3)$. This trend illustrates the decreasing ability of the directional water–molecule interactions to produce local tetrahedral order, the perfect version of which yields precisely four nearest neighbors. The same trend is also clear from the increasing ratio of distances for second and first $g_{OO}^{(2)}$ maxima: $1.63(T_1)$, $1.69(T_2)$, $1.83(T_3)$; in the ideal ice lattice the ratio is $2\sqrt{2}/\sqrt{3}=1.633$. Both sets of numbers probably converge toward values appropriate to a fluid with central forces only and equivalent packing density (e.g., supercritical argon[12]).

Figure 4 exhibits the three computed radial pair correlation functions $g_{OH}^{(2)}$ for unlike nuclei in different molecules, and Fig. 5 gives analogous results for $g_{HH}^{(2)}$. Although these functions provide structural views of the water model independent of that represented by $g_{OO}^{(2)}$, the same trend as before emerges: Increasing the temperature at fixed density causes a significant reduction in local molecular correlation. Evidently this reduction demonstrates increasing defection from ideal hydrogen-bonding distances and orientations, so at extremely high temperatures $T \gg T_3$ no remanent influence of the discrete set of nuclear pair distances for ice should appear.

B. Polyhedral Correlation Resolutions

In order to achieve a more vivid description of local order in our water model than can be provided by radial pair correlation functions alone, explicit information about molecular orientational arrangement is necessary. Reference 1 included a resolution of $g_{OO}^{(2)}$ for T_2 into three sectorial components,

$$g_{OO}^{(2)}(r)=g_{I}(r)+g_{II}(r)+g_{III}(r), \qquad (2.4)$$

which were generated by the faces of a regular icosahedron. This polyhedron was imagined to be centered at an oxygen nucleus, and oriented so that the four tetrahedral directions emanating from that nucleus, which would form undistorted hydrogen bonds, simultaneously pass through the centroids of four noncontiguous faces. Figure 6(a) shows these four triangular faces by shading. Directly opposite these four "class I" faces are four others or "class III" faces. The remaining 12 faces, denoted "class II" share edges each with faces of the other two classes.

The component g's indicated in Eq. (2.4) represent populations of other oxygen nuclei, viewed from the position of the one at the icosahedron center, through the triangular "windows" of types I–III. The geometric character of ordinary hexagonal ice (as well as its cubic modification) suggests that this resolution is an apt one, for in these locally tetrahedral crystals, first neighbors will appear only in g_I, second neighbors only in g_{II}, and g_{III} will receive contributions only from neighbors of third or higher orders. The degree to which these ice restrictions are violated in the liquid measures the degree of hydrogen-bond distortion.

The regular octahedron provides an even simpler (but less discriminating) way to resolve $g_{OO}^{(2)}$. As Fig. 6(b) indicates, four of its eight faces can have centroids simultaneously pierced by the tetrahedral directions. These nonadjacent faces will be denoted by "IV," and the remaining four faces by "V." Hence

$$g_{OO}^{(2)}(r)=g_{IV}(r)+g_{V}(r). \qquad (2.5)$$

In a defect-free ice lattice, first neighbors to the central oxygen will appear only in g_{IV}, while g_V can contain contributions from higher-order neighbors only.

Figures 7(a) and 7(b) compare the triplet of functions g_I, g_{II}, g_{III} for the two extreme temperatures T_1 and T_3. Figure 8 does the same for g_{IV} and g_V. Both comparisons clearly illustrate the decreasing local "ice-likeness" attendant upon increase in temperature. As

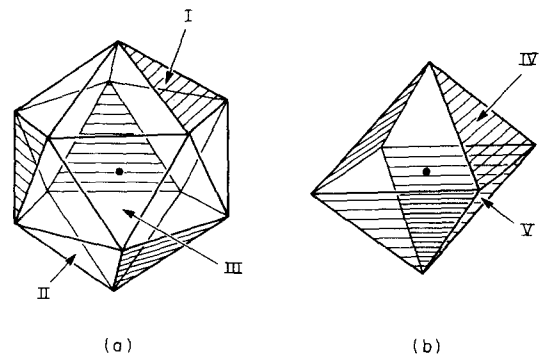

FIG. 6. Polyhedral bases for orientational resolution of $g_{OO}^{(2)}$. The four shaded faces for both the icosahedral (a) and octahedral (b) schemes are those whose centers may simultaneously be pierced by a tetrahedral set of directions (i.e., undistorted H bonds). Single examples of the face classes are indicated by Roman numerals.

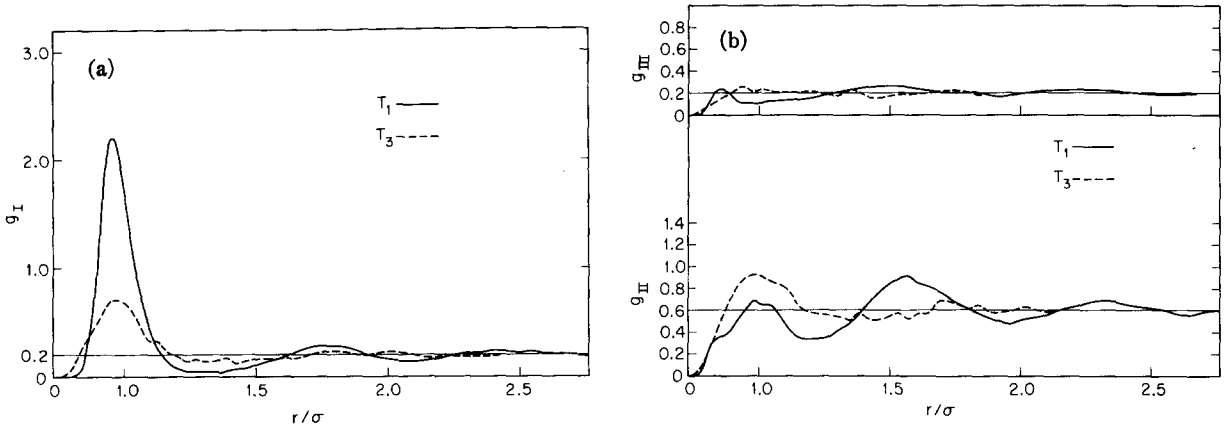

FIG. 7. (a) Icosahedrally resolved pair correlation functions. The component shown at T_1 and T_3 refers to face I in Fig. 6(a). (b) Icosahedrally resolved pair correlation functions. The components shown for T_1 and T_3 refer to faces II and III in Fig. 6(a).

T increases toward infinity, all of the five functions should become more and more nearly proportional to one another.

More elaborate polyhedral resolutions of course are possible; for example each icosahedron vertex in Fig. 6(a) could be truncated to add 12 pentagonal faces, making 32 faces in all.[13] In the limit, a full spherical resolution would be achieved. At present these generalizations are statistically inconvenient—not enough data are available for such fine resolutions.

C. Dipole Direction Correlations

The polyhedral resolutions (2.4) and (2.5) do not in themselves specify how the dipole directions (the symmetry axes) of neighboring molecules are correlated. However, this aspect of orientational order also can be revealed by suitable further computations. Let $\boldsymbol{\mu}_i^{(1)}$ be the unit vector directed along the permanent dipole moment direction of molecule i, and define

$$\mathbf{M}=\sum_{i=1}^{216}\boldsymbol{\mu}_i^{(1)}. \tag{2.6}$$

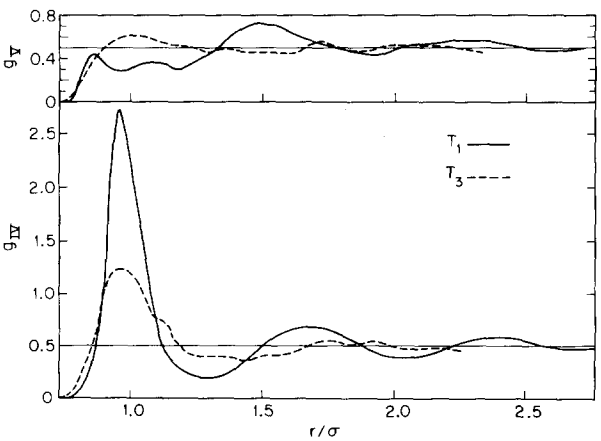

FIG. 8. Octahedrally resolved pair correlation functions, g_{IV} and g_V.

Then the quantity

$$G_K=\langle M^2\rangle/N \tag{2.7}$$

would equal unity if the molecular dipole directions were entirely uncorrelated. However it was noticed earlier[1] that the positive quantity G_K tends to be substantially less than unity; our computations lead to the values,

$$G_K(T_1)=0.20,$$
$$G_K(T_2)=0.171,$$
$$G_K(T_3)=0.278. \tag{2.8}$$

(The first of these is somewhat uncertain due to sluggishness of molecular motion at low temperatures.) The degree of cancellation between moments of interacting molecules is obviously quite significant, even at T_3.

The static dielectric constant ϵ_0 of a polar fluid depends upon the correlation in orientation of neighboring molecular dipoles. The Kirkwood theory of polar dielectrics[14] provides the following expression for ϵ_0:

$$(\epsilon_0-1)(2\epsilon_0+1)/3\epsilon_0=4\pi\rho[\alpha+(\mu_1^2 g_K/3k_BT)]; \tag{2.9}$$

here ρ is the number density, α is the molecular polarizability, μ_1 is the liquid-phase molecular dipole moment, and k_B is Boltzmann's constant. The Kirkwood orientational correlation factor g_K includes (besides self-correlation) contributions from all neighbors, weighted according to the cosine of the angle between dipole directions. In terms of the full orientation- and position-dependent pair correlation function $g^{(2)}(\mathbf{x}_1, \mathbf{x}_2)$, in the infinite system limit, we have[1,2]

$$g_K=1+(\rho/8\pi^2)\int d\mathbf{x}_2(\boldsymbol{\mu}_1^{(1)}\cdot\boldsymbol{\mu}_2^{(1)})g^{(2)}(\mathbf{x}_1, \mathbf{x}_2). \tag{2.10}$$

The present molecular dynamics calculations are not capable of determining ϵ_0. But since it has been established[1] that

$$g_K=[(\epsilon_0+2)(2\epsilon_0+1)/9\epsilon_0]G_K, \tag{2.11}$$

TABLE II. Dielectric properties at the three sets of scaled temperatures employed in Table I. For comparison with the liquid-phase dipole moments μ_l, the isolated molecule moment $\mu_v = 1.84$ D.

$\zeta =$	0.00	0.03	0.06	0.09
T_1(°C)	−8.2	−0.2	7.7	15.7
G_K(m.d.)	0.20			
ϵ_0(exptl)[a]	91.09	87.82	84.71	81.69
g_K	4.16	4.01	3.88	3.74
μ_l(D)	1.94	1.97	1.99	2.02
T_2(°C)	34.3	43.5	52.8	62.0
G_K(m.d.)	0.171			
ϵ_0(exptl)[a]	75.07	72.00	69.03	66.21
g_K	2.95	2.83	2.72	2.61
μ_l(D)	2.25	2.28	2.31	2.34
T_3(°C)	314.8	332.4	350.1	367.7
G_K(m.d.)	0.278			
ϵ_0(exptl)[b]	32	30	29	28
g_K	2.13	2.01	1.95	1.89
μ_l(D)	2.35	2.38	2.41	2.43

[a] C. G. Malmberg and A. A. Maryott, J. Res. Natl. Bur. Std. **56**, 1 (1956).

[b] E. U. Franck, Pure Appl. Chem. **24**, 13 (1970).

we can use measured ϵ_0 values along with our computed G_K's to evaluate the Kirkwood factor g_K. The results have been gathered in Table II, with the same temperature assignments that appear in Table I. Once having established g_K, the Kirkwood formula (2.9) may be utilized to evaluate μ_l, with results that are also entered in Table II. We do not agree with Minton's suggestion[15] that *both* g_K and μ_l should decline as T increases (only the former does); whether this disagreement indicates inadequacy of our model or not requires further study.

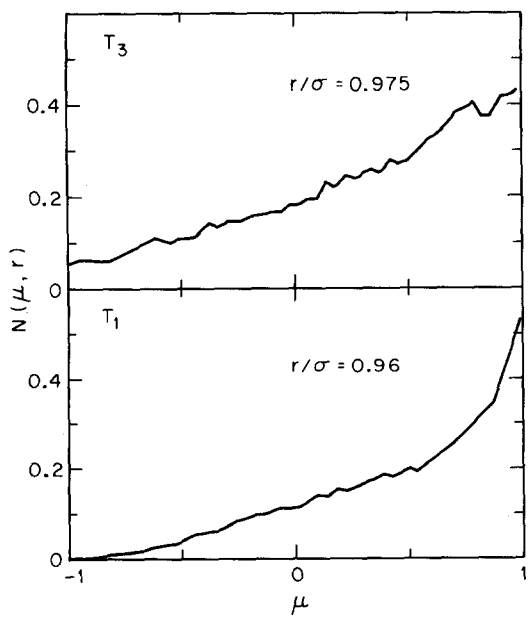

FIG. 9. Dipole direction correlation function $N(\mu, r)$ at the first-neighbor distance.

It appears that contributions to the integral, in the defining expression (2.10) for g_K, are not uniform in sign from all shells of neighbors. Figures 9 and 10, respectively, show $N(\mu, r)$ for the first and second neighbor distances (defined in terms of $g_{OO}^{(2)}$ maxima); this function gives the probability for a neighbor (2) at distance r from a fixed molecule (1) to be oriented so that the cosine of the angle between the dipole directions is μ:

$$\mu = \boldsymbol{\mu}_1^{(1)} \cdot \boldsymbol{\mu}_2^{(1)}. \tag{2.12}$$

Clearly first neighbors tend to have parallel alignment,

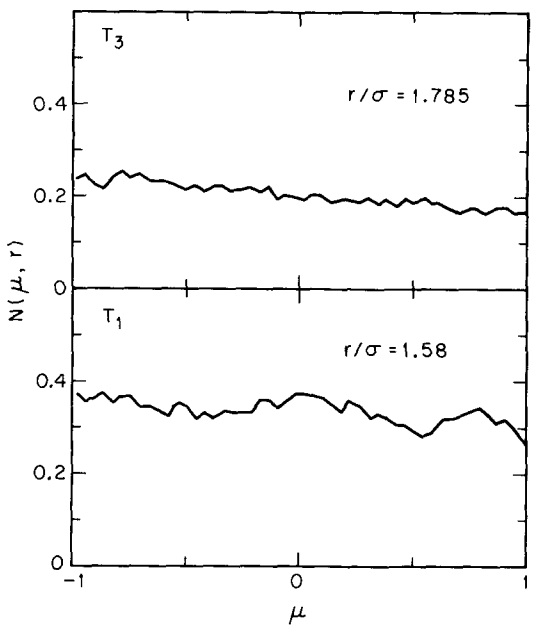

FIG. 10. Dipole direction correlation function $N(\mu, r)$ at the second-neighbor distance.

whereas second neighbors tend to be antiparallel. As with all correlations, the effect weakens with increasing temperature.

D. Bond Energy Distribution

We denote by $p(V)$ the density in energy of neighbors with which a given molecule experiences mutual interaction potential equal to V. This density may be expressed in terms of the full pair correlation function $g^{(2)}(\mathbf{x}_1, \mathbf{x}_2)$ in the following manner:

$$p(V) = (\rho/8\pi^2) \int d\mathbf{x}_2 \delta[V - V_{\text{eff}}^{(2)}(\mathbf{x}_1, \mathbf{x}_2)] g^{(2)}(\mathbf{x}_1, \mathbf{x}_2). \tag{2.13}$$

At very low temperature $p(V)$ should exhibit discrete classes of molecular pairs resulting from the regular crystallographic pattern in ice. Obviously $p(V)$ will always vanish for V less than the absolute minimum of $V_{\text{eff}}^{(2)}$, which for the unscaled potential lies at -6.50 kcal/mole.

The three densities $p(V)$ for T_1, T_2, and T_3 are jointly shown in Fig. 11. The divergence at $V=0$ (proportional to V^{-2} in an infinite system) is a temperature-independent feature that merely indicates the existence of many pairs at large separation interacting weakly as dipoles. Although Fig. 11 specifically refers to the unscaled potential ($\zeta=0$), conversion to general ζ only requires multiplying abscissa readings by $1+\zeta$.

The most notable feature in Fig. 11 is the near invariance of $p(V)$ to temperature change for $V\cong-3.5$ kcal/mole.[16] This apparent invariance point V_0 is reminiscent of the isosbestic points that appear in Raman spectra of water at different temperatures. We suggest that both may be due to the presence of a single basic excitation mechanism. This mechanism involves rupture of the bond between molecular pairs below V_0, to leave those pairs with energy finally above V_0.

The average potential energy increase which *all* molecular pairs undergo due to thermal excitation will be

$$\Delta V=\int_{-\infty}^{+\infty} V\left(\frac{\partial p(V,T)}{\partial T}\right)dV \Big/ \int_{(+)}\left(\frac{\partial p(V,T)}{\partial T}\right)dV, \tag{2.14}$$

where the denominator integral only spans those V intervals for which

$$\partial p(V,T)/\partial T>0. \tag{2.15}$$

By using the molecular dynamics data at T_1 and T_2 to form a finite-difference approximation to $\partial p/\partial T$ in Eq. (2.14), we obtain the numerical result for the 216-particle system,

$$\Delta V\cong 0.95 \text{ kcal/mole}. \tag{2.16}$$

This mean energy increase contains a strong contribution from the redistribution of the many pairs near $V=0$: The peak in $p(V)$ is more biased toward small negative V at low temperatures than it is at high temperatures. In the infinite system limit this effect overwhelms ΔV and forces it to vanish.

It is also important to note from Fig. 11 that the depletion region $-6.50<V<V_0$ roughly counterbalances the accretion region just above V_0, i.e., $V_0<V<-1.44$. The fundamental excitation process of hydrogen-bond breakage should thus correspond to the transfer of a pair initially within the first of these regions to the second region. The centroids of these regions lie, respectively, at -4.98 and -2.44 kcal/mole (calculated from the T_1 and T_2 curves). The difference between centroid positions, 2.54 kcal/mole, can tentatively be identified as the average energy required to break a

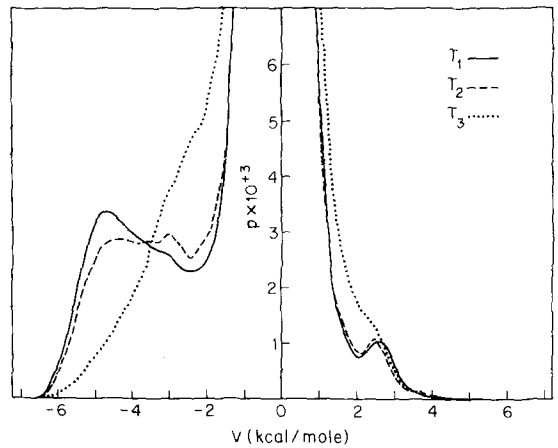

FIG. 11. Pair interaction density in liquid water. The energies shown refer to the unscaled potential ($\zeta=0$).

hydrogen bond in our model. Of course this breakage normally begins with a somewhat strained hydrogen bond, and ends with a more weakly interacting pair to be sure, but one still stabilized by $V_{\text{eff}}^{(2)}$ relative to $V=0$. Under rescaling of the potential, the average hydrogen bond breakage energy naturally must be multiplied by $1+\zeta$.

It is significant that this energy has the same magnitude as experimentally determined heats of hydrogen-bond breakage. On the basis of his Raman studies, Walrafen[17] obtains 2.55 kcal/mole. Infrared spectra taken by Worley and Klotz[18] imply the comparable value 2.4 kcal/mole. In addition Davis and Litovitz[19] have argued that a two-state interpretation of the thermodynamic properties of liquid water requires about 2.6 kcal/mole for bond breakage. Recently, Bucaro and Litovitz[20] have inferred a heat of 2.5 ± 0.1 kcal/mole for this process from depolarized light scattering measurements. Our suggestion that these heats can all arise from a bond excitation process across V_0 is strengthened by observation of chronological sequences of stereophotographs of intermediate configurations from the molecular dynamics runs; both bonded and unbonded (dangling) OH groups persist as such for many vibrational periods.

The energy V_0 leads to an unambiguous division of pairs into "hydrogen bonded" and "non-hydrogen bonded." More generally we can introduce a variable cutoff energy V_{HB}, to employ the more flexible division:

$$\begin{aligned} &V_{\text{eff}}^{(2)}(i,j)<V_{\text{HB}} \qquad (i,j \text{ hydrogen bonded}),\\ &V_{\text{eff}}^{(2)}(i,j)\geq V_{\text{HB}} \qquad (i,j \text{ not hydrogen bonded}). \end{aligned} \tag{2.17}$$

Irrespective of whether V_{HB} is selected to equal V_0 or not, an interesting new category of questions immediately arises about how these bonds are distributed geometrically in the liquid, and what variations ar

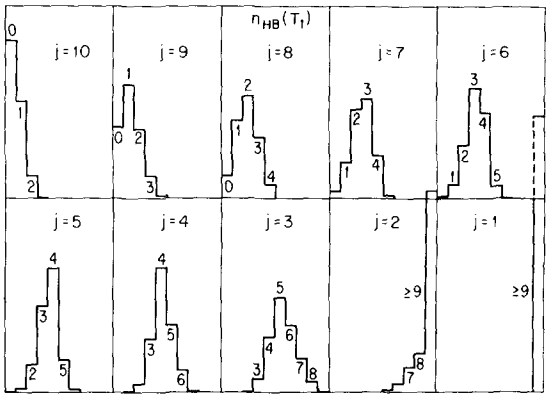

FIG. 12. Distribution of molecules by hydrogen-bond number at T_1. Index j refers to potential cutoff choice, $V_{HB}(j)$, defined in Eq. (2.18).

brought about by temperature changes. It might, for instance, be valuable to know the relative concentrations of closed hydrogen-bond polygons of 4, 5, 6, 7, ···sides, and how they link to one another in three-dimensional networks.

Up to the present we have only undertaken the less ambitious task of inquiring how many molecules engage in precisely n hydrogen bonds ($n=0, 1, 2, \cdots$), for several alternative V_{HB} choices,

$$V_{HB}(j)=-8(j-1)\epsilon$$
$$=-0.5768(j-1)\ \text{kcal/mole}. \quad (2.18)$$

The invariant point V_0 of $p(V)$ corresponds closely to $V_{HB}(7)=-3.461$ kcal/mole. The respective distributions of hydrogen bond numbers for T_1, T_2, and T_3 are provided by Figs. 12–14 in histogram form. In each case the distributions remain singly peaked as $V_{HB}(j)$ varies. Indeed the distributions are roughly similar from one temperature to the next after a shift in V_{HB}: To obtain approximately the same distribution at higher temperature, a larger V_{HB} is required. There is, however, a slight tendency toward greater breadth at higher temperature.

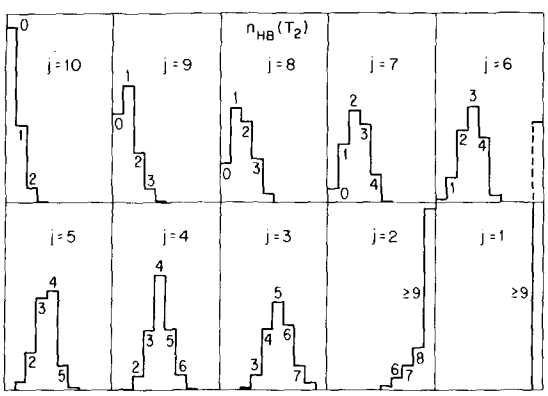

FIG. 13. Distribution of molecules by hydrogen-bond number at T_2.

Owing to the fact that the distributions in Figs. 12–14 are all singly peaked, we can extend to all temperatures our earlier observation for T_2[1] that the molecular dynamics calculations conflict with those "two-state theories" of water which divide molecules dichotomously into "bonded" vs "unbonded." We include in this set of theories those that postulate bulky icelike clusters,[21,22] self-clathrates,[23] and distorted ice models with interstitials.[24–26]

In order to provide a more complete picture of our hydrogen-bond breakage mechanism, separate molecular energies should eventually be calculated for molecules engaging in different numbers of hydrogen bonds, using V_0 as the cutoff. We would expect to find a common difference in these energies about equal to $\frac{1}{2}(2.54\ \text{kcal/mole})=1.27$ kcal/mole. Furthermore, these common differences should be nearly independent of temperature, in spite of the fact that the distributions shown in Figs. 12–14 are not. Findings of this character

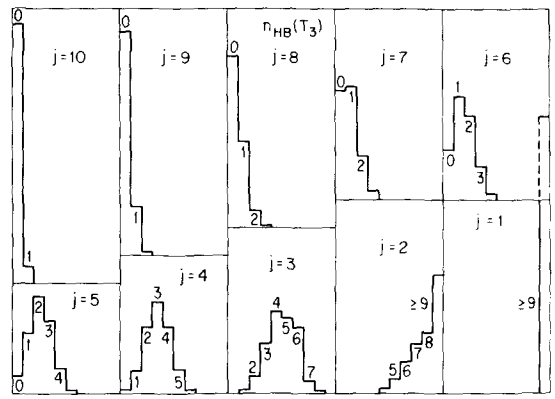

FIG. 14. Distribution of molecules by hydrogen-bond number at T_3.

could then serve as the basis for a "mixture model" of liquid water, which would then supplant the questionable "two-state theories" alluded to above.[21–26]

III. TEMPERATURE EFFECTS ON KINETICS

If change in mean molecular velocity were the only way that constant-volume temperature variations were to affect kinetic properties of a fluid, then those properties would scale in a trivial way with T. This would be the case, for example, if the molecules behaved mechanically as elastic rigid spheres. Relaxation times would then be proportional to $T^{-1/2}$, while the self-diffusion constant D and the shear viscosity η would vary as $T^{1/2}$. Measured transport properties for liquid water near room temperature on the other hand show far more rapid variations with T. These rapid variations reflect the marked extent to which the random hydrogen-bond network in the liquid changes its character with temperature. The molecular dynamics calculations reveal similar behavior.

A. Self-Diffusion

Two alternative routes to the self-diffusion constant D are available. The first follows from the mean-square value of the molecular center-of-mass displacement $\Delta\mathbf{R}_j(t)$, at long times t,

$$D\sim\langle[\Delta\mathbf{R}_j(t)]^2\rangle/6t. \tag{3.1}$$

The other involves the autocorrelation function for molecular center-of-mass velocity $\mathbf{v}_j$; again for large t,

$$D\sim\frac{1}{3}\int_0^t\langle\mathbf{v}_j(0)\cdot\mathbf{v}_j(t')\rangle dt'. \tag{3.2}$$

In an infinite system, t could be allowed to approach infinity, and it is a trivial matter to show that the expressions (3.1) and (3.2) are then equivalent. For a molecular dynamics run of limited duration involving a finite system, they are *not* equivalent; the available dynamical information is weighted differently by the two expressions. For reasons of stability in results, we consider (3.1) in the present context to be the more reliable approach. However as longer dynamical runs on water soon become available, equivalence should be restored.

Table I presents values of D obtained via Eq. (3.1) for all three molecular dynamics runs with several ζ

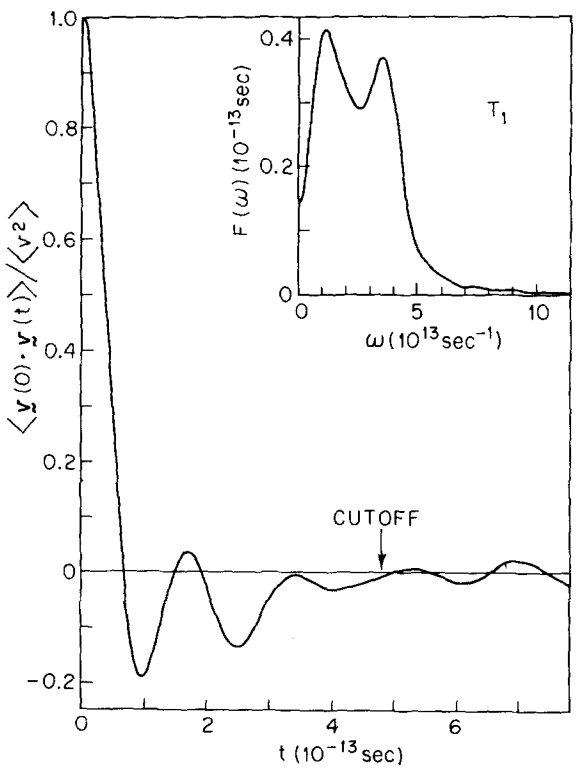

FIG. 15. Velocity autocorrelation function for center-of-mass motion at T_1. The inset shows the corresponding power spectrum (Fourier transform) $F(\omega)$. The "cutoff" locates the time beyond which noise due to incomplete phase averaging dominates; the autocorrelation function should in fact be close to zero in that region. The time scale refers to $\zeta=0$.

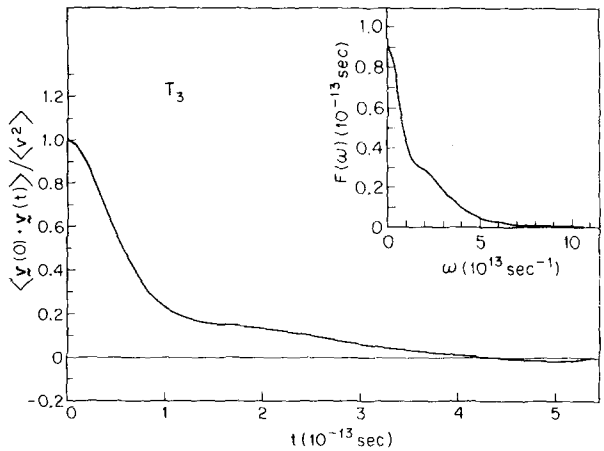

FIG. 16. Velocity autocorrelation function for center-of-mass motion at T_3. The inset shows the corresponding power spectrum $F(\omega)$. The time scale refers to $\zeta=0$.

choices. By comparison with the direct experimental values for D that are available in the T_1, T_2 range,[27] it would appear that $\zeta=0.06$ provides a desirable rescaling of the interaction. If this specific rescaling magnitude is adopted, our water model seems successful in reproducing the rapid temperature variation experimentally observed for D.

The principal virtue of the velocity autocorrelation functions $\langle\mathbf{v}_j(0)\cdot\mathbf{v}_j(t)\rangle$ is the short-time detail they reveal about typical molecular diffusive motions. Figures 15 and 16, respectively, present these functions computed at T_1 and T_3.[28] They are obviously very different. At the low temperature T_1 the molecules are surely subject to considerable oscillation, but only the slightest hint of that oscillation remains at T_3. Appropriately positioned and oriented neighbors are present at T_1 to hold a molecule in place to some extent. At T_3 by contrast the molecular arrangements manifest far less local network rigidity.

In the low-temperature range (T_1 and T_2) the oscillatory character of molecular motion does not imply that diffusion proceeds by occasional jumps between discrete binding sites ("quasicrystalline lattice sites"). As stressed previously,[1] it is more accurate to describe typical motions as a vacillating tour in the strong force field of the constantly changing network pattern.

The motion at T_3 seems not to be grossly different from those observed for rigid spheres at about half the close-packed density.[29] Evidently the orientation-dependent part of the pair interaction continuously loses effectiveness, compared to repulsive molecular core forces, as T rises.

Power spectra $F(\omega)$ for the velocity autocorrelation functions are shown as insets in Figs. 15 and 16. The most prominent characteristic of the T_1 spectrum is the pair of maxima at 1.2×10^{13} sec^{-1} and 3.6×10^{13} sec^{-1} (i.e., at frequencies 64 and 191 cm^{-1}). Almost certainly these "modes" should be identified with the broad intermolecular bands observed by Raman, infra-

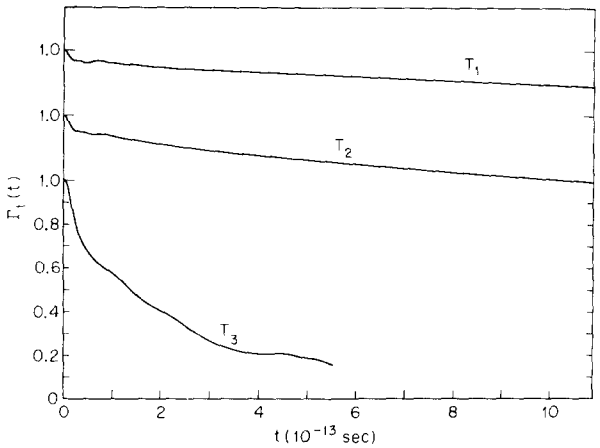

FIG. 17. Dipole direction correlation function $\Gamma_1(t)$ for the three temperatures T_1, T_2, and T_3. The time scale is appropriate for the unscaled interaction.

red, and neutron spectroscopy to be centered around 60 and 170 cm^{-1}, respectively, in real water.[30] The higher frequency of these two "modes" perhaps involves the oscillation of a molecule in an unbroken hydrogen-bond "cage" of neighbors, and hence involves bond stretching. The lower frequency on the other hand could result from simultaneous motion of several bonded molecules forming a chain, for example, whose movement involves bond bends or rotations at less energy cost than stretch. In any event, the higher frequency "mode" is considerably subdued at T_2 (see Ref. 1, Fig. 22), and neither is visible at T_3.

In principal there is nothing to prevent the molecular dynamics method from investigating a strongly supercooled water sample, perhaps not inappropriately to be identified as a glass. The corresponding velocity auto correlation function should be no less oscillatory than the one shown in Fig. 15, and would probe the vibrational spectrum for that rigid amorphous structure.

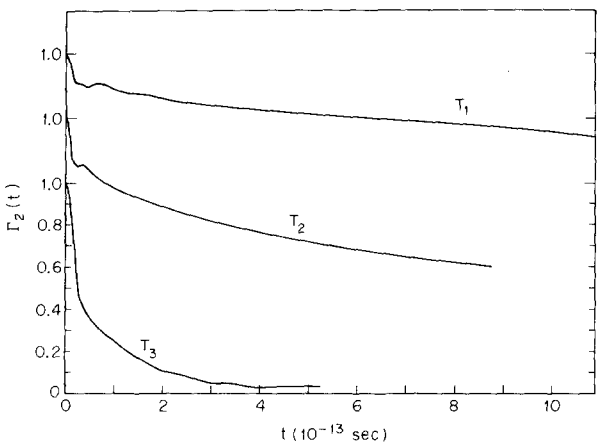

FIG. 18. Dipole direction correlation function $\Gamma_2(t)$. The time scale refers to the unscaled interaction.

B. Rotational Relaxation

One way to examine the rotational motions executed by the molecules is to calculate the quantities:

$$\Gamma_n(t) = \langle P_n[\cos\theta_j(t)]\rangle, \tag{3.3}$$

where $\theta_j(t)$ is the angle through which the dipole direction of molecule j turns in time t, and where P_n is the usual Legendre polynomial. Figure 17 shows Γ_1 at the three temperatures T_1, T_2, and T_3, while Fig. 18 does the same for Γ_2.

As might have been anticipated from the self-diffusion constants for our model, it is obvious that rotational motion proceeds much more freely at high temperature than at low temperature. The incomplete phase averaging forced upon us by finite runs makes the Γ_1 and Γ_2 curves less smooth than they should be at large t; within that imprecision it is probably appropriate to presume that simple exponential behavior obtains in the Γ_n after the initial librational oscillation dies away.[31] This exponential regime is observed only in its initial stages at T_1 due to severely hindered motion, and only slightly more at T_2. At T_3, on the other hand, virtually all of the Γ_1 and Γ_2 decays are observed.

TABLE III. Dipole relaxation times, in picoseconds. The τ_1 and τ_2 refer to autocorrelation functions Γ_1 and Γ_2, while τ_d is the real water dielectric relaxation time, measured[34] at T_1 and T_2, and estimated from viscosities for T_3.

$\zeta=$	0.00	0.03	0.06	0.09
T_1(°C)	−8.2	−0.2	7.7	15.7
τ_1	8.9	8.8	8.6	8.5
τ_2	3.6	3.5	3.5	3.4
τ_d	24.2	18.0	13.7	10.8
T_2(°C)	34.3	43.5	52.8	62.0
τ_1	5.6	5.5	5.4	5.4
τ_2	2.1	2.1	2.0	2.0
τ_d	6.7	5.5	4.6	3.9
T_3(°C)	314.8	332.4	350.1	367.7
τ_1	0.34	0.34	0.33	0.33
τ_2	0.21	0.21	0.20	0.20
τ_d	...	...	...	...

The apparent exponential relaxation times τ_1 and τ_2 corresponding to Γ_1 and Γ_2 are listed in Table III, with the previously considered ζ options. These times are probably accurate only to within 20%.

Although τ_1 is intimately related to the macroscopic dielectric relaxation time τ_d, there is as yet no consensus about the precise connection. For high-dielectric-constant polar fluids, Powles[32] claims that

$$\tau_d = 3\tau_1/2, \tag{3.4}$$

whereas Nee and Zwanzig[33] suggest that

$$\tau_d = 2\tau_1. \tag{3.5}$$

Comparison with measured τ_d [34] that are also included in Table III shows that both (3.4) and (3.5) are consistent with a small positive ζ for T_1 (though our τ_1 determination is somewhat uncertain at this temperature), but not for T_2. A more definitive comparison must await development of a dielectric relaxation theory specifically designed to describe highly structured liquids such as water.

For classical rotational diffusion, τ_1/τ_2 would be precisely 3. The entries in Table III show within available precision a downward drift of this ratio as temperature rises. This is the result expected as the molecular rotations become less and less hindered.

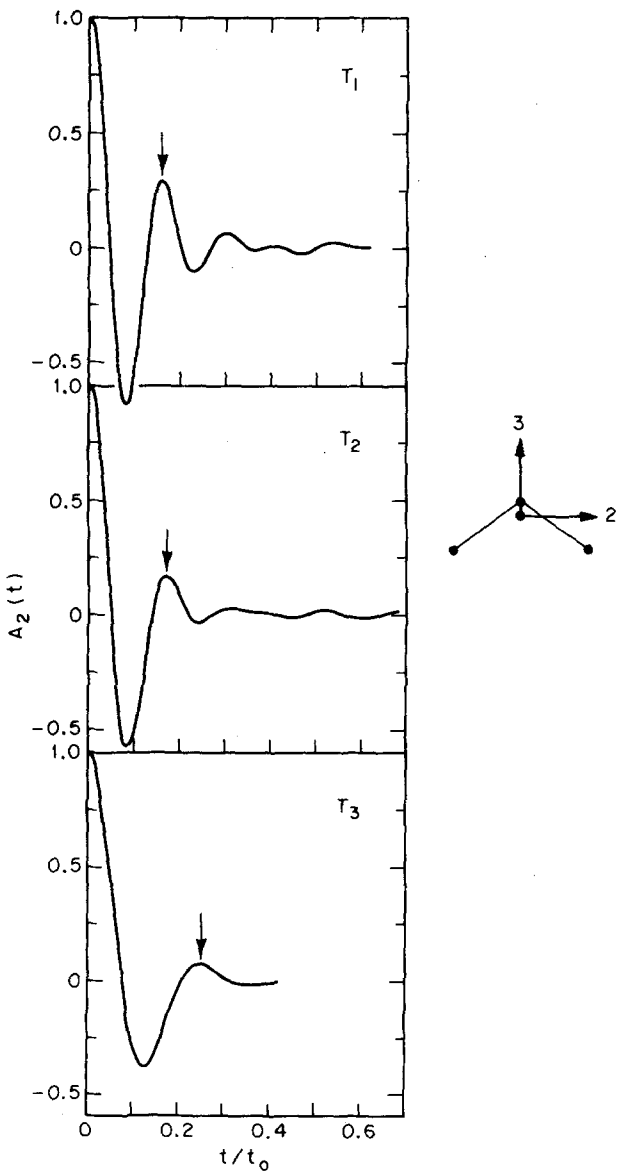

FIG. 19. Normalized angular momentum autocorrelation functions. The rotation axis lies in the molecular plane, perpendicular to the dipole axis, and corresponds to the smallest of the inertial moments. For unscaled interactions ($\zeta=0$), $t_0=2.1775\times10^{-13}$ sec.

Figure 19 compares normalized angular momentum autocorrelation functions,

$$A_\alpha(t) = \langle \omega_\alpha(0)\omega_\alpha(t)\rangle / \langle \omega_\alpha^2 \rangle, \tag{3.6}$$

at T_1, T_2, and T_3 for that rotational component ($\alpha=2$) corresponding to the least of the molecular inertial moments. The rotation axis for this component lies in the molecular plane, perpendicular to the dipole axis. The librational motion about this axis is faster than motions about the other two axes, so it provides a convenient probe of the force field of neighbors before those neighbors are able to move very much.

The time (for $\zeta=0$) at which the first maximum in $A_2(t)$ occurs, for $t>0$, shifts from 3.5×10^{-14} sec at T_1 to 5.5×10^{-14} sec at T_3. This increase shows clearly how thermal disruption moves neighbors out of optimal positions and orientations to bind the central molecule.

IV. DISCUSSION

In order to supplement the constant-volume temperature variations studied here, it would be valuable to investigate the structural influence of strong compression. At 75°C, real water may be compressed to about 20 kbar before it solidifies into ice VI, and under that pressure its density has increased to approximately 1.30 g/cm^3. If two molecular dynamics runs were carried out at the same temperature 75°C, but at the contrasting densities 1.00 and 1.30 g/cm^3, it would be possible to compare the ways in which $g_{OO}^{(2)}$, for example, changed with T and pressure p. Although it has sometimes been suggested that increases in T and in p are similar "structure breaking" influences,[35] the molecular dynamics approach would likely be capable of resolving relatively subtle differences in their respective effects.

Although the evidence presented in Table I indicates that rescaling of our potential with $\zeta\approx0.06$ improves representation of water at room temperature somewhat, there is obviously room for further improvement. Surely that will require more basic changes in the potential than can be produced merely by rescaling.

There is evidence in our results that the interaction used is too tetrahedral, i.e., the hydrogen bonding is too directional. The average value of the configurational part of C_V (the heat capacity at constant volume) between temperatures T_1 and T_2 may be calculated from mean interaction energies $\langle V_N \rangle$ in Table I to be 21.4 cal/mole·deg; experimentally the value is only 11 cal/mole·deg. By interpreting these magnitudes in terms of relative rise rates of entropy with temperature, we see that structural order in our model breaks up more rapidly than it should. Favorable bonding possibilities that are too restrictive in angles of relative orientation could easily produce this effect, since they

would strongly confine motion at low T_1 and be relatively ineffective at high T where the only type of hydrogen bond that could reasonably exist would involve severe distortion.

The radial pair correlation functions $g_{HH}^{(2)}$ shown in Fig. 5 display suspicious shoulders at small distance, showing the existence of hydrogen pairs even closer than the intramolecular pair. Undoubtedly these pairs of positive point charges [see Eq. (1.1)] which by themselves repel, are simultaneously bound and stabilized by the *same* negative point charge at the back of a third molecule. In the case of real water molecules the unshared electron pairs are much more delocalized, and close hydrogen-pair encounters would be less frequent.

When two molecules in our model have their protons simultaneously bound to a negative point charge of a third, there will be a tendency for their oxygens to be jammed rather closely together. The functions $g_{OO}^{(2)}$ in Figs. 1–3 seem to possess weak shoulders inside the first-neighbor peak maximum, that perhaps also result in this way from overemphasized tetrahedrality. The small-distance behavior of the polyhedral resolutions supports this identification.

In order to mitigate this shortcoming in our potential, some sort of negative charge delocalization is mandatory. As we have previously remarked,[1] one way to accomplish this involves shortening the distance between each oxygen nucleus and its negative point charges. Whether or not this will suffice to produce a dramatically improved representation of real water can be judged only through the hindsight afforded by the correspondingly modified molecular dynamics calculations. Nevertheless we believe that the present crude simulation already achieves proper qualitative description of the real liquid, and further work will produce refinements only in quantitative detail.

ACKNOWLEDGMENTS

A portion of the T_1 computation was carried out at the IBM Computation Center, New York City. We are grateful to Dr. Seymour Koenig for arranging this grant of computer time.

* Part of the work carried out at the Argonne National Laboratory was supported by the U.S. Atomic Energy Commission.

[1] A. Rahman and F. H. Stillinger, J. Chem. Phys. **55,** 3336 (1971).

[2] A. Ben-Naim and F. H. Stillinger, "Aspects of the Statistical-Mechanical Theory of Water," in *Structure and Transport Processes in Water and Aqueous Solutions*, edited by R. A. Horne (Wiley-Interscience, New York, 1972).

[3] K. Morokuma and L. Pederson, J. Chem. Phys. **48,** 3275 (1968).

[4] P. A. Kollman and L. C. Allen, J. Chem. Phys. **51,** 3286 (1969).

[5] J. Del Bene and J. A. Pople, J. Chem. Phys. **52,** 4858 (1970).

[6] D. Hankins, J. W. Moskowitz, and F. H. Stillinger, J. Chem. Phys. **53,** 4544 (1970).

[7] G. H. F. Diercksen, Theoret. Chim. Acta. **21,** 335 (1971).

[8] $\epsilon = 5.01 \times 10^{-15}$ erg $= 7.21 \times 10^{-2}$ kcal/mole, $\sigma = 2.82$ Å.

[9] $R_L = 2.0379$ Å, $R_U = 3.1877$ Å.

[10] F. H. Stillinger, J. Phys. Chem. **74,** 3677 (1970).

[11] For the purpose of making this estimate, we have extrapolated data given in: T. Grindley and J. E. Lind, Jr., J. Chem. Phys. **54,** 3983 (1971).

[12] W. W. Wood, "Monte Carlo Studies of Simple Liquid Models," in *Physics of Simple Liquids*, edited by H. N. V. Temperley, J. S. Rowlinson, and G. S. Rushbrooke (Wiley, New York, 1968), pp. 223–224.

[13] These 32 faces are equivalent to the zones into which the surface of a conventional soccer ball is partitioned.

[14] J. G. Kirkwood, J. Chem. Phys. **7,** 911 (1939).

[15] A. P. Minton, Chem. Phys. Letters **7,** 606 (1970).

[16] The magnitude of our statistical error at present is comparable to the small differences shown between the curves in Fig. 11 at $V = -3.5$ kcal/mole.

[17] G. E. Walrafen, in *Hydrogen-Bonded Solvent Systems*, edited by A. K. Covington and P. Jones (Taylor and Francis, London, 1968), pp. 9–29.

[18] J. D. Worley and I. M. Klotz, J. Chem. Phys. **45,** 2868 (1966).

[19] C. M. Davis, Jr., and T. A. Litovitz, J. Chem. Phys. **42,** 2563 (1965).

[20] J. A. Bucaro and T. A. Litovitz (to be published).

[21] H. S. Frank and W. Y. Wen, Discussions Faraday Soc. **24,** 133 (1957).

[22] G. Némethy and H. A. Scheraga, J. Chem. Phys. **36,** 3382 (1962).

[23] L. Pauling, in *Hydrogen Bonding*, edited by D. Hadzi and H. W. Thompson (Pergamon, New York, 1959), pp. 1–5.

[24] M. D. Danford and H. A. Levy, J. Am. Chem. Soc. **84,** 3965 (1962).

[25] O. Ya. Samoilov, *Structure of Aqueous Electrolyte Solutions and the Hydration of Ions* (Consultants Bureau, New York, 1965).

[26] J. W. Perram, Mol. Phys. **20,** 1077 (1971).

[27] D. C. Douglass and K. T. Gillen (to be published).

[28] See Ref. 1, Fig. 22 for the T_2 autocorrelation function, which differs only in minor quantitative detail from that for T_1 shown here in Fig. 15.

[29] B. J. Alder and T. Wainwright, in *Transport Processes in Statistical Mechanics*, edited by I. Prigogine (Interscience, New York, 1958), p. 119.

[30] These intermolecular bands are discussed at length by G. E. Walrafen, in *Water: A Comprehensive Treatise, Volume I. Physics and Physical Chemistry of Water*, edited by F. Franks (Plenum, New York, 1972).

[31] With the precision and time intervals currently available, we cannot detect the nonexponential hydrodynamic "tails" that should arise in autocorrelation functions at long times; see (a) B. J. Alder and T. E. Wainwright, Phys. Rev. A **1,** 18 (1970), (b) M. H. Ernst, E. H. Hauge, and J. M. J. van Leeuwen, Phys. Rev. Letters **25,** 1254 (1970), (c) N. K. Ailawadi and B. J. Berne, J. Chem. Phys. **54,** 3569 (1971).

[32] J. G. Powles, J. Chem. Phys. **21,** 633 (1953).

[33] T.-W. Nee and R. W. Zwanzig, J. Chem. Phys. **52,** 6353 (1970).

[34] D. Eisenberg and W. Kauzmann, *The Structure and Properties of Water* (Oxford U. P., New York, 1969), p. 207.

[35] Reference 34, Sec. 4.3.